

## Classical Quantum Gravity

Crossmark

ARTICLE

RECEIVED  
dd Month yyyy  
REVISED  
dd Month yyyy

## Calibrating spectral siren cosmology with synthetic catalogs of binary black hole mergers

Arianna Scarpa<sup>1\*</sup>, Simone Mastrogiovanni<sup>1</sup> , Filippo Santoliquido<sup>2,3</sup> , Manuel Arca Sedda<sup>2,3,4</sup> <sup>1</sup>INFN, Sezione di Roma, I-00185 Roma, Italy <sup>2</sup>Gran Sasso Science Institute, Via F. Crispi 7, I-67100 L'Aquila, Italy <sup>3</sup>INFN, Laboratori Nazionali del Gran Sasso, I-67100 Assergi, Italy <sup>4</sup>INAF, Osservatorio Astronomico di Roma, I-00040 Monte Porzio Catone (Rome), Italy

\*Author to whom any correspondence should be addressed.

**E-mail:** arianna.scarpa@ligo.org**Keywords:** cosmic expansion history, gravitational-wave, BAO, cosmology, spectral siren, non-parametric inference**Abstract**

Binary black hole (BBH) mergers detected through Gravitational Waves (GWs) are a promising probe for the cosmic expansion. These sources are standard sirens for which we can directly measure the luminosity distance, but their redshift is degenerate with the determination of their source masses. In analogy to standard candles, the redshift of standard sirens can be obtained using a calibration based on the source mass spectrum, but without the need for a cosmological ladder. It has been recently shown that a mismodeling of the BBH mass spectrum is very likely to introduce a bias in the determination of the Hubble constant. To tackle this issue, we develop a BBH population model based on Normalizing Flows, trained on synthetic BBH catalogs generated from astrophysical prescriptions, including binaries formed through both isolated stellar evolution and dynamical environments. We validate this approach with a mock BBH dataset, demonstrating that the Normalizing Flow framework faithfully recovers the true distribution and eliminates systematic biases in the Hubble constant inference. By using this model on GWTC-4.0 data, we obtain  $H_0 = 71.62^{+4.04}_{-4.00}$  kms<sup>-1</sup>Mpc<sup>-1</sup> at 68.3% credible interval. Assuming the astrophysical prescriptions present in B-POP, we also show that the determination of  $H_0$  is degenerate with the fraction of binaries born in the dynamical and isolated formation channel, with a Planck cosmology favouring  $\sim 35\%$  binaries formed in the dynamical environment while a SH0ES cosmology favouring a value of  $\sim 25\%$ .

**1 Introduction**

Gravitational Wave (GW) sources are rapidly becoming promising probes of the cosmic expansion. This is particularly relevant given the unresolved puzzle in modern cosmology known as the ‘‘Hubble tension’’ [1]: measurements of the Hubble constant  $H_0$  differ between direct measurements in the local Universe and indirect estimates based on early universe observations from the Cosmic Microwave Background [2].

GWs from compact binary coalescences (CBCs) provide a direct measurement of the luminosity distance to the source, without the need for cosmological ladder [3, 4], unlike standard candles such as supernovae [5]. However, they do not provide a direct estimation of the redshift that could be obtained from the identification of the source host galaxy as in the case of GW170817 [6, 7]. When no electromagnetic counterpart is detected, the source redshift can be inferred statistically, either by using the source frame mass properties - also known as spectral siren method - of binary black holes (BBHs) [8–16], galaxy catalogs [17], or cross-correlation [4, 18–23] with large-scale structure tracers.

With the release of the fourth Gravitational Wave Transient Catalog (GWTC-4.0) [24], the LIGO-Virgo-KAGRA (LVK) collaboration has confirmed that the mass distribution of BBHs is one of the most promising avenues to measure the cosmic expansion [25]. The mass spectrum of BBHs is far from trivial [26] to describe; it can contain under density and overdensity of BBH production. These features might arise from the astrophysical formation mechanisms of BBHs. Population studies are becoming increasingly precise thanks to the rapidly growing number of detections. Despite these advances, population modeling remains a major challenge, as modeling compact

binary formation channels is intrinsically complex. Recent works have highlighted tensions in the literature regarding correlations between binary parameters such as mass, spin and redshift [27–31] and this is because BBH populations are expected to belong to distinct astrophysical formation channels and to change at different cosmic times because of metallicity and stellar evolution processes [32, 33]. The current GW inference on cosmological parameters makes use of phenomenological prescriptions [26] to describe the BBH population. This approach is currently named “strongly modelled”. Analytical phenomenological models such as Power Laws and Gaussian Peaks could not capture the complex behaviour of the BBH mass spectrum. To solve this issue, a possible solution is to employ non-parametric or semi-analytical models for the mass distribution [16, 34–36]. However, these models do not capture the redshift evolution of the mass distribution, and this mismodeling is shown to introduce systematic biases in the inferred value of the Hubble constant  $H_0$  [37–40].

This work directly addresses this issue by introducing a non-parametric population model calibrated on state-of-the-art population synthesis simulations of BBHs. Catalogs of BBHs naturally include all the correlations between masses, redshift, and other binary parameters that could arise from astrophysical formation channels. The non-parametric models that we consider are Normalizing Flows. These are powerful machine learning neural network capable of learning complex probability distributions directly from data, without imposing analytical functional forms. This flexibility is shown to be required for unbiased cosmological inference, but it can also be exploited to infer population information and thus to connect astrophysical simulations of BBH to GW observations. More generally, normalizing flows have been employed in recent works to emulate astrophysical simulations and to perform population inference from GW catalogs [41–45].

This paper is organized as follows. In Sec 2 we introduce the hierarchical Bayesian inference framework, the spectral sirens method and the non-parametric population model based on Normalizing Flows. In Sec. 4 we validate the model using a mock catalog with a redshift-evolving population. In Sec 5 we apply the model to an astrophysical synthesis catalog and to simulated and real gravitational wave observations, jointly constraining cosmological and population parameters. Our findings are finally summarized in Sec 6.

## 2 Hierarchical Bayesian Inference and Normalizing Flows

In this section we introduce the hierarchical Bayesian inference framework and the non-parametric population model based on Normalizing Flows.

### 2.1 Hierarchical Bayesian inference

Inference of cosmological and population parameters from GW observations is performed within the framework of hierarchical Bayesian inference (HBI) [46–48], in which the CBCs detection process is modeled as an inhomogeneous Poisson process. In this work, the analyses are implemented in the ICAROGW pipeline [49]. Given a set of observed gravitational wave data  $\{x_i\}$ , the likelihood for the population parameters  $\Lambda$  is given by the so-called *hierarchical likelihood*:

$$\mathcal{L}(\{x\}|\Lambda) \propto e^{-N_{\text{exp}}(\Lambda)} \prod_{i=1}^{N_{\text{obs}}} T_{\text{obs}} \int \mathcal{L}(x_i|\theta, \Lambda) \frac{dN}{d\theta dt}(\Lambda) d\theta, \quad (1)$$

where  $\theta$  represents the binary parameters,  $\mathcal{L}(x_i|\theta, \Lambda)$  is the single-event likelihood, and  $T_{\text{obs}}$  is the observation time.  $N_{\text{exp}}(\Lambda)$  represents the expected number of detected events and accounts for selection effects. It is defined as:

$$N_{\text{exp}}(\Lambda) = T_{\text{obs}} \int \frac{dN}{d\theta dt}(\Lambda) d\theta \int_{x \in \text{detectable}} \mathcal{L}(x_i|\theta, \Lambda) dx. \quad (2)$$

The integral over detectable events represents the probability that a signal with parameters  $\theta$  is detected, and it accounts for the selection bias [50] caused by the finite sensitivity of gravitational wave detectors.

The population model enters the hierarchical likelihood through the detector-frame rate  $\frac{dN}{d\theta dt}$ , which depends on cosmological parameters and on the population parameters that describe the intrinsic properties of the sources. This method is the so-called *spectral sirens* analysis [51], in which cosmological information is extracted from gravitational wave observations by exploiting the relation between the detector-frame and source-frame parameters, without the need of an electromagnetic redshift measurement. The detector-frame rate is usually factorized as:

$$\frac{dN}{dL dm_{1d} dm_{2d} dt_d} = R_0 p_{\text{pop}}(m_{1s}, m_{2s}|\Lambda, z) \Psi(z, m_{1s}, m_{2s}|\Lambda) \frac{dV_c}{dz} \frac{1}{1+z} \frac{1}{|J_{d \rightarrow s}|}, \quad (3)$$

where  $R_0$  is the local merger rate density,  $p_{\text{pop}}(m_{1s}, m_{2s}|\Lambda, z)$  and  $\Psi(z, m_{1s}, m_{2s}|\Lambda)$  are the distributions describing the joint primary and secondary source-frame mass distributions and the redshift evolution of the merger rate, respectively. The factor  $dV_c/dz$  is the differential comoving volume element, while the term  $1/(1+z)$  and the Jacobian  $|J_{d \rightarrow s}|$  account for the conversion from detector-frame to source-frame parameters.

In most GW population analyses,  $p_{\text{pop}}$  is assumed to be redshift-independent and  $\Psi$  is assumed to be masses-independent. If the mass distribution is assumed to be independent of redshift, then the intrinsic shape of the BBH mass spectrum does not evolve with cosmic time. Indeed it is specified through phenomenological parametric models: the population parameters  $\Lambda$  determine the shape of the distribution using fixed analytical prescriptions such as Power Laws and Gaussian peaks or Broken Power Law models [26, 52]. When such redshift evolution is not taken into account, the mismatch between the true population and the assumed phenomenological model can lead to systematic biases in hierarchical inference [37–40]. This limitation motivates the need for a non-parametric population model that does not rely on analytical functions fixed in redshift, but instead learns the joint BBH source-frame mass and merger redshift distribution directly from astrophysical synthesis catalogs, consistently incorporating redshift-dependent mass evolution within the HBI framework.

In the following, we introduce a non-parametric model for  $p_{\text{pop}}$  and  $\Psi$  based on the machine learning technique of Normalizing Flows, which allows us to describe the joint distribution of BBH source-frame masses and merger redshift without using phenomenological prescriptions. In this approach, the factorization of the source-frame mass and merger redshift probability densities is replaced by a single joint probability density:

$$p_{\text{pop}}(m_{1s}, m_{2s}|\Lambda, z)\Psi(z, m_{1s}, m_{2s}|\Lambda) = k p_{\text{NF}}(m_{1s}, m_{2s}, z). \quad (4)$$

where  $p_{\text{NF}}(m_{1s}, m_{2s}, z)$  is the joint probability density function (pdf) computed with the NF and it is normalized such that  $\int p_{\text{NF}} dm_{1s} dm_{2s} dz = 1$ , and  $k$  is an overall normalization factor that converts the pdf into the corresponding physical merger rate. This formulation directly models correlations between BBH source-frame masses and merger redshift. The model is trained on astrophysical BBH synthesis catalogs to consistently incorporate redshift-dependent mass evolution within the HBI framework. This approach is extended in a scenario where we are provided with catalogs reporting difference formation channels. In this case, we can define a mixture fraction  $\phi$  [53] such that

$$p_{\text{NF}}(m_1, m_2, z) = \phi p_{\text{NF}}^{\text{A}}(m_1, m_2, z) + (1 - \phi) p_{\text{NF}}^{\text{B}}(m_1, m_2, z), \quad (5)$$

where A, B indicate two separate formation channels. The mixture fraction is a population parameter of the hierarchical likelihood.

## 2.2 Non-parametric population model: Normalizing Flows

NF [54–56] are generative machine learning models that allow us to compute complex probability density functions through invertible and differentiable transformations between a latent distribution and the observable parameter space. In this work, the latent variable  $u \in \mathbb{R}^3$  is drawn from a multivariate standard Gaussian distribution  $p_U(u) = \mathcal{N}(0, \mathbb{I})$  and mapped to the observable variables  $x = (m_{1s}, m_{2s}, z)$  through an invertible transformation  $x = f(u)$ . The resulting probability density is obtained with the change-of-variables formula:

$$p_X(x) = p_U(f^{-1}(x)) |\det J_{f^{-1}}(x)| = p_U(u) |\det J_f(u)|^{-1}, \quad (6)$$

where  $J_{f^{-1}}$  is the Jacobian of the inverse transformation.

The transformation  $f$  is built with the ZUKO library, using Neural Spline Flows (NSF) [57], in which the mapping is parametrized by autoregressive, monotonic rational-quadratic spline transformations [58]. More details about the NF’s architecture, renormalization and training are given in App. A.2. NFs provide the flexibility needed to capture such complex distributions of BBH masses and merger redshift. This allows us to construct a non-parametric estimate of the full joint distribution  $p_{\text{NF}}(m_{1s}, m_{2s}, z)$ .

## 3 Calibration of the NF model

In this section, we describe the procedure used to choose the hyper parameters of the Normalizing Flows model, which are discussed together with the NF architecture, in Appendix A.2. We perform a grid search varying the number of transformation layers, the number of hidden neurons, the learning rate and the batch size. For each configuration, when the NF is trained on a catalog, the

negative log likelihood (NLL) is minimized on the training set and the corresponding validation loss is evaluated. The selection of the final model is not based only on the minimum validation loss: different architectures often yield to very similar NLL (that differ up to 5%) but we find that their performance in hierarchical inference is not. Models with the lowest NLL fit the overall distribution better, but they not always recover the injected values of  $H_0$  and  $\phi$  that are used when we generate mock GW observations from the catalogs. This is because small discrepancies in the low-redshift tails, that is where GW observations lie, can affect the recovery of the injected values. We thus rank the configurations according to their validation loss, computed as the weighted average of the losses of the two formation channels. Then, we select the first  $N$  best-performing architectures and we validate them within the HBI framework with mock GW observations from the BBH synthetic catalog: the model that recovers the injected  $H_0$  and  $\phi$  within 90% C.I. are kept and the lightest structure is chosen, to minimize computational times. This procedure is a required calibration step for the NF population model, the goal is to identify the best-performing NF that provides unbiased and reliable cosmological inference.

#### 4 Benchmark of the model on a mock catalog

To test whether the NF can correct the systematic bias in the  $H_0$  inference, we build a redshift-evolving mock BBH source population, and then simulate GW observations from it and infer  $H_0$ . We consider two different scenarios: first, we adopt a phenomenological population model that does not evolve with redshift; second, we use the NF model to fit BBH source-frame masses and merger redshift samples drawn from the redshift-evolving population. This benchmark have been also used to calibrate the architecture of the normalizing flow as reported in App. A.2.

The redshift-evolving source-frame population is given by a POWER LAW + EVOLVING PEAK model as the one employed in [40], in which the mean of the Gaussian Peak evolves linearly with redshift. The population parameters used to generate the mock catalog are chosen to be in agreement with the ones inferred from the GWTC-3.0 analyses [52, 59] and are reported in Appendix A.1. The astrophysical distribution of primary masses and merger redshift in the mock catalog is shown in Fig. 1, where the linear evolution of the Gaussian Peak is clearly visible. The fraction of GW events in the Evolving Peak is set to  $\phi = 0.08$ , following Eq. 5. We note that, throughout this benchmark, the Power Law and Evolving Peak components should be interpreted as phenomenological representatives of two distinct formation channels and are combined through the mixture coefficient  $\phi$ . However, in standard GW analyses [25, 26],  $\phi$  has no direct physical interpretation in terms of formation channels and it simply parametrizes the fraction of events in the peak.

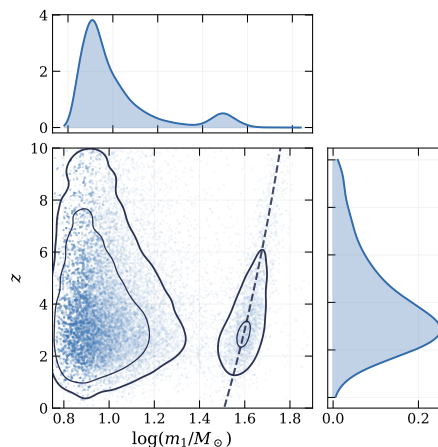


**Figure 1.** Astrophysical distribution of the mock BBH source-frame drawn from the POWER LAW + EVOLVING PEAK population, used to benchmark the model. The plot is shown in the  $\log m_1 - z$  plane, where the dots are samples drawn from the redshift-evolving distribution. Contour lines enclose the 68% and 90% density regions. The dashed line shows the linear redshift evolution of the mean of the Gaussian Peak:  $\mu(z) = z \mu_{z_1} + \mu_{z_0}$ . The top and right panels show the corresponding marginal distributions.

Mock GW observations are generated by reweighting a set of detected injections in O3 detectors data [60] according to a POWER LAW + EVOLVING PEAK population. The cosmological parameters are fixed to  $H_0 = 67.7 \text{ km s}^{-1} \text{ Mpc}^{-1}$  and  $\Omega_m = 0.308$  [61]. This procedure consistently accounts for GW selection effects under the assumed population model. For this benchmark, we assume that we can perfectly measure the detector masses and luminosity distance of the GW

source. This is an unrealistic assumption for real data, but it is a useful benchmark to control, even in the most optimistic scenario, if NF can be employed for redshift-evolving mass distributions.

In the first test case, we model the mass distribution with a POWER LAW + PEAK, thus ignoring the redshift evolution. We infer  $H_0$  using the Markov chain Monte Carlo (MCMC) technique, fixing the matter density parameter to  $\Omega_m = 0.308$  and using a uniform prior on the Hubble constant  $H_0 \sim \mathcal{U}(20, 120) \text{ km s}^{-1} \text{ Mpc}^{-1}$ . We fix the rest of the population parameters to their true values reported in App. A.1, setting the redshift-evolution parameter to  $\mu_{z_1} = 0$ . The  $H_0$  posterior distribution is shown in Fig. 2 and reproduces the systematic bias already reported in the literature [40],  $H_0$  can be found at the 99.7% interval. The analytical form of the POWER LAW + PEAK phenomenological model, which does not evolve with redshift, is the origin of the bias. This implies that whenever a redshift-evolving population is modelled using a population that is fixed in redshift, a systematic error arises from the mismatch between the true population and the phenomenological approximation. Contrary, as we can see from Fig. 2, NFs are capable of approximating the catalog of GW sources and recover a posterior that includes the simulated  $H_0$  value.

In the second test case, we model the mass using two different NFs linked with a mixture fraction  $\phi$  as in Eq. 5. The first population is composed of all the GW events generated from the Power Law, while the second is composed of the GW events generated by the Redshift-Evolving Peak, both populations and their NF fits are shown in Fig. 3. As in the previous case, we infer  $H_0$  fixing  $\Omega_m = 0.308$  and the mixture coefficient to its injected value  $\phi = 0.08$  and assuming a uniform prior on the Hubble constant  $H_0 \sim \mathcal{U}(20, 120) \text{ km s}^{-1} \text{ Mpc}^{-1}$ . Results are shown in Fig. 2, the systematic bias on  $H_0$  is fully corrected thanks to the Normalizing Flows, which accurately fit the redshift-evolving population.

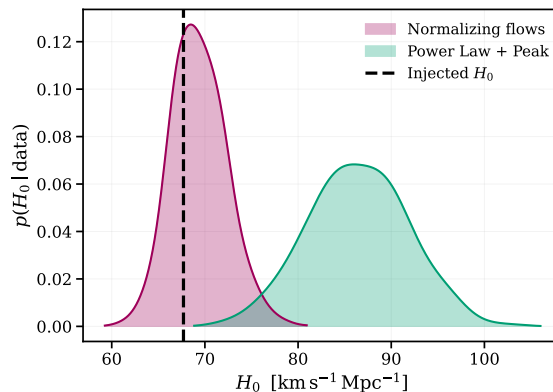


**Figure 2.** Posterior distributions of  $H_0$  inferred using the mock GW catalog under two different population assumptions. The purple posterior is obtained when masses are modeled with the phenomenological POWER LAW + PEAK that does not evolve with redshift: the injected value of  $H_0$  (vertical dashed line) falls outside the 99.7% C.I. of the inferred posterior. The magenta posterior shows inference results obtained using Normalizing Flows to fit the redshift-evolving population: the evolution is well captured and the injected  $H_0$  value is recovered.

## 5 Application to a synthetic BBH catalog: Calibration and analysis on GWTC-4.0

We now consider a synthetic astrophysical catalog generated with the B-POP pipeline [62], which provides an astrophysically motivated description of the BBH population across cosmic time. The population realization includes contributions from the isolated binary evolution formation channel and dynamically formed channels (globular clusters, nuclear clusters, and young clusters) [32]. The B-POP population model predicts that BBHs formed in the dynamical formation channel account for the 37% of the population while the ones from isolated formation channels account for 63%. For each channel, the source-frame primary and secondary masses, the merger redshift, together with the redshift merger rate  $R(z)$  per unit comoving volume and source-frame time, are provided and correspond to one year. B-POP [63–66] generates mock BBH populations in synthetic Universes that are uniquely defined by the cosmological star formation history of galactic fields and star clusters — young, globular, and nuclear clusters — the redshift evolution of stellar metallicity, the dynamical evolution of star clusters, the stellar evolution of single and binary stars, the natal mass and spin distribution, and spin alignment, of stellar BHs. In this work, we adopt the fiducial model described in Arca Sedda et al (2026). We refer the reader to B-POP latest paper for more details about the code and the model.

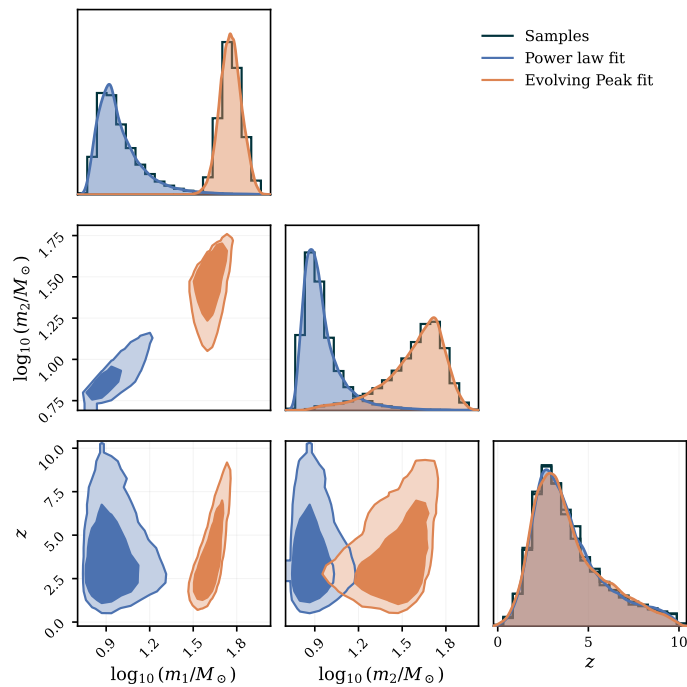


**Figure 3.** Corner plot showing the joint distribution of BBH masses and merger redshift for the two mock populations. Blue and orange contours (enclosing the 68.3% and 90% credible regions) and smoothed KDE curves represent the normalizing flow fits for the Power Law and the Evolving Peak, respectively. Grey histograms, shown only in the one-dimensional marginals, correspond to samples drawn from the mock redshift-evolving catalog. The Normalizing Flows accurately recover the underlying mass and redshift distributions for both channels.

The B-POP population is characterized by a complex mass spectrum featuring sharp structures and a strong redshift evolution. Indeed, at different cosmic times, we expect different BBH populations; thus, the redshift evolution is intrinsically embodied in the simulated catalog. This behavior can be seen in Fig. 4, which shows the evolution of the primary BBH mass across redshift bins. Such complexity cannot be modeled using analytical phenomenological parametrizations, but it can be fitted using a Normalizing Flows model. Before using a NF trained on B-POP to analyze

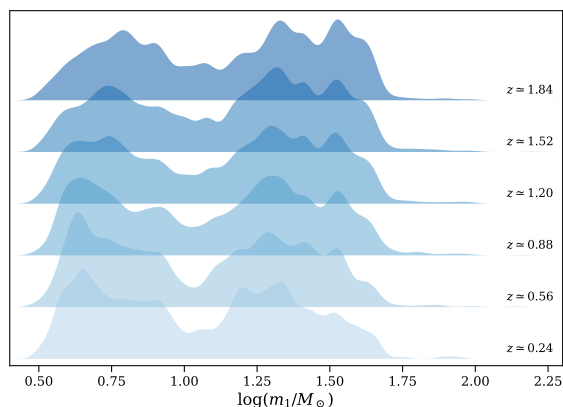


**Figure 4.** Redshift evolution of the primary BBH mass distribution in the synthetic astrophysically simulated B-POP catalog. Each curve shows the distribution of  $\log(m_1/M_\odot)$  within a redshift bin. The population has a complex, multimodal structure and a strong redshift dependence. This complex behavior cannot be modeled with analytical phenomenological laws but can be captured using Normalizing Flows.

GW events from GWTC-4.0, we perform a study with mock data to test the chosen architecture of the NF.

### 5.1 Calibration of the NF

We generate a synthetic set of 700 GW observations from the B-POP catalog [67, 68] in an O5-like era [67, 69] by mapping the BBH parameters to detector-frame quantities, fixing cosmology to

$H_0 = 67.7 \text{ km s}^{-1} \text{ Mpc}^{-1}$  and  $\Omega_m = 0.308$ . We decided to use an O5-like scenario, as its increased sensitivity will allow us to detect a fraction of the B-POP population significantly larger than the one detectable in O4. As such, a NF calibrated for an O5-like observing scenario would suffice to approximate a population detectable in O4.

As a metric for the GW detection, we use a proxy for the signal-to-noise ratio (SNR) model defined as:

$$\rho = \rho_0 \theta \left( \frac{\mathcal{M}_d}{\mathcal{M}_{d,0}} \right)^{5/6} \frac{d_{L,0}}{d_L} S(f_{\text{isco}}(m_{1d}, m_{2d})), \quad (7)$$

where  $\mathcal{M}_d$  is the detector-frame chirp mass,  $d_L$  is the luminosity distance, and  $\theta$  encodes the geometric projection of the source relative to the detector network. The reference values  $\mathcal{M}_{d,0}$  and  $d_{L,0}$  are fixed according to [67] to reproduce a O5-like detector network. The function  $S(f_{\text{isco}}(m_{1d}, m_{2d}))$  suppresses contributions from extremely massive BBH mergers whose inspiral ends at frequencies below  $\sim 20$  Hz. Such events can be found in the high-mass tail of the B-POP catalog and would otherwise produce artificially large SNRs; this effect is regularized by the function  $S$ , which downweights these events. The uncertainties on the measurement of the detector masses and luminosity distance for each event, are generated using toy likelihood models as described in [67]. We denote the set of 700 GW observations, and their error budgets on masses and distances, as parameter estimation samples. Using the same framework, we also generate a set of  $10^8$  detectable GW signals to evaluate the selection effects as described in [49].

For this analysis, we consider two effective formation channels on which we train two NFs: isolated binary evolution and dynamical formation in dense stellar environments. Each channel is modeled independently using a NF trained on the BBH mass and redshift distributions. The details of the NF's architecture are given in App. A.2. Figure 5 shows the joint distributions of BBH source-frame masses and merger redshift for the two formation channels and the corresponding normalizing flow fits of the B-POP population. The normalizing flow model correctly recovers the mass spectrum and its evolution with redshift. We then define the detector-frame rate used for

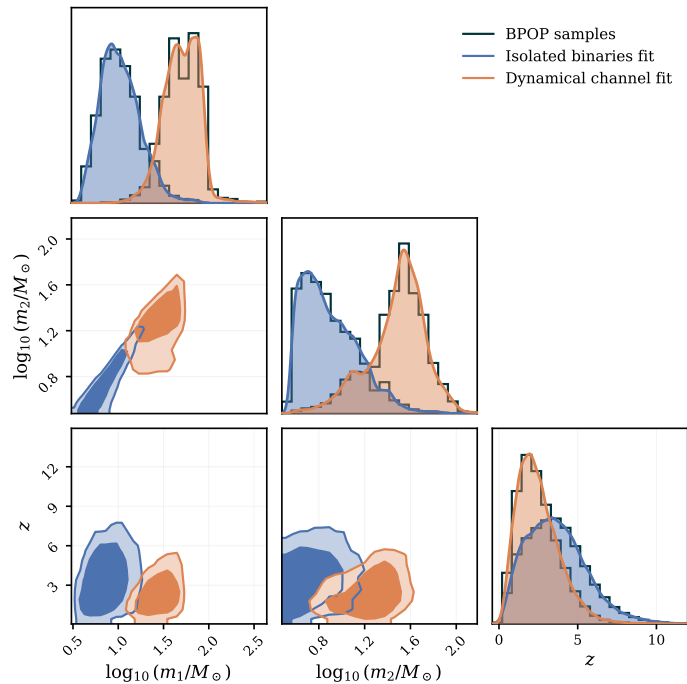


**Figure 5.** Corner plot showing the joint distribution of BBH primary and secondary masses and merger redshift for the two formation channels. Blue and orange contours (that enclose the 68.3% and 90% credible regions) and smoothed kde curves show the normalizing flow fits of the isolated binary and dynamical channels, respectively. Grey histograms show the B-POP population samples and are shown only in the one-dimensional marginals. The Normalizing Flows fits correctly recover the mass and redshift spectra for both channels.

hierarchical Bayesian inference as:

$$\frac{dN}{dd_L dm_{1d} dm_{2d} dt_d} = \left[ (1 - \phi) p_{\text{NF}}^{\text{iso}}(m_{1s}, m_{2s}, z) + \phi p_{\text{NF}}^{\text{dyn}}(m_{1s}, m_{2s}, z) \right] \frac{dV_c}{dz} \frac{1}{1+z} \frac{1}{|J_{d \rightarrow s}|} \frac{N_{\text{astro}}}{T_{\text{obs}}}. \quad (8)$$

Here, the observing time is set to  $T_{\text{obs}} = 1 \text{ yr}$  and the number of astrophysical BBH merger follows Eq 13 and it is equal to  $N_{\text{astro}} = 6.6 \times 10^4 \text{ events/yr}$ , as predicted by B-POP. Further details on

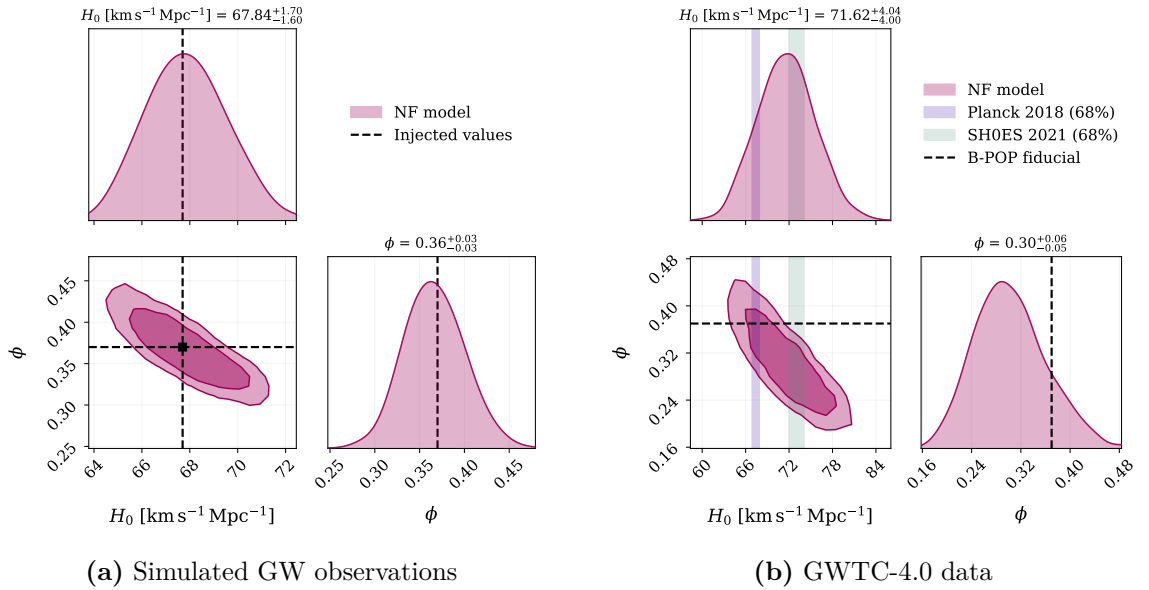


**Figure 6.** Joint posterior distributions of the Hubble constant  $H_0$  and the mixture fraction of the dynamical BBH formation channel  $\phi$ . (a) Inference performed on simulated GW data generated from the B-POP catalog using an MCMC sampler. Dashed lines indicate the injected values used to generate simulated data. Posteriors are compatible with the injected data, showing the correct fit of the Normalizing Flows to the B-POP population. (b) Constraints inferred from GWTC-4.0 data using a nested sampling algorithm within the same population model adopted for the simulated data. Vertical bands indicate the 68% credible intervals from Planck 2018 (violet) and SHOES 2021 (green); the dashed line shows the B-POP fiducial value  $\phi = 0.37$ . In both panels, the contours enclose the 68.3% and 90% credible regions, and the diagonal panels show the marginalized one-dimensional posteriors.

the detector rate are given in Appendix A.3. In the above prescription,  $\phi$  is the fraction of binaries formed in the dynamical formation channel. Using Eq. 2, we estimate the number of expected detections,  $N_{\text{exp}} = 691 \pm 26$ , which is compatible within the 68.3% credible interval with the number of the 700 simulated parameter estimation samples.

The simulated GW observations are used to perform hierarchical Bayesian inference on the Hubble constant  $H_0$  and the dynamical formation channel mixture fraction  $\phi$ . We use a uniform prior for the Hubble constant  $H_0 \sim \mathcal{U}(20, 120) \text{ km s}^{-1} \text{ Mpc}^{-1}$  and for the mixture fraction  $\phi \sim \mathcal{U}(0, 1)$ , while the matter density parameter is fixed to  $\Omega_m = 0.308$  [61]. The joint posterior distribution is shown in Fig. 6(a): the injected values of  $H_0$  and  $\phi$  are recovered with no evidence for systematic biases. This demonstrates that the Normalizing Flows population model provides an accurate non-parametric representation of the fiducial B-POP catalog.

### 5.2 Analysis on GWTC-4.0

We apply the population model, validated on the simulated data, to real gravitational-wave observations from the GWTC-4.0 catalog, using the 153 detected events with inverse false alarm rate  $\text{IFAR} > 1 \text{ yr}$  [24]. To correct for selection biases, we use a set of software injections recovered by low-latency pipelines in real O3 and O4a data [70]. For the analysis, we use the rate model as written in Eq. 8, where the two normalizing flows are the same as the one benchmarked during the calibration. We firstly note that, using the reported  $R(z)$  from B-POP, we would expect  $N_{\text{exp}} = 163 \pm 12$  detections, which are consistent with the size of the observed catalog.

The joint posterior distribution inferred using GWTC-4.0 data is shown in Fig. 6(b), it was obtained using a uniform prior for the Hubble constant  $H_0 \sim \mathcal{U}(20, 120) \text{ km s}^{-1} \text{ Mpc}^{-1}$  and for the mixture fraction  $\phi \sim \mathcal{U}(0, 1)$ , while the matter density parameter was fixed to  $\Omega_m = 0.308$  [61]. The constraints on  $H_0$  and  $\phi$  are broader than those obtained from simulated observations because of the limited number of detected events and current detector sensitivity. The inferred value of  $H_0 = 71.62_{-4.00}^{+4.04} \text{ km s}^{-1} \text{ Mpc}^{-1}$  is consistent, within uncertainties, with both early- and late-Universe measurements [2, 5] the mixture fraction  $\phi = 0.30_{-0.05}^{+0.06}$  is compatible within the 90% credible interval with the fiducial B-POP population,  $\phi = 0.37$ .

We note that the precision of  $H_0$  that we obtain is significantly more precise than the one reported in the latest GWTC-4.0 cosmological studies [25]. However, this is not surprising, as in our analysis, we are fixing the population model to the BBH population described by B-POP, with the only additional degree of freedom being the mixture fraction between BBHs formed in dynamical

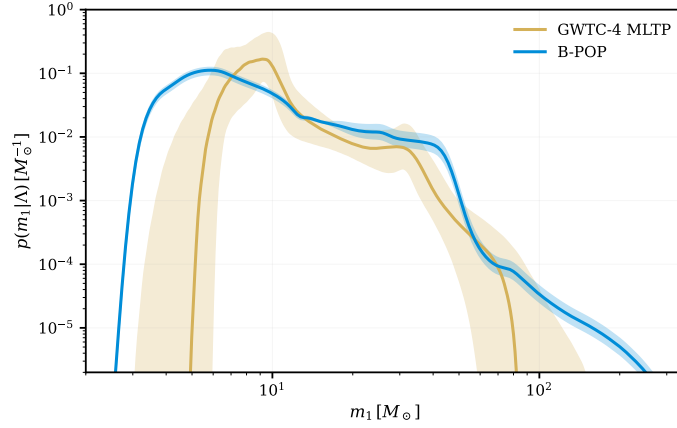


**Figure 7.** Primary source mass distribution  $p(m_1)$ , reconstructed from the fiducial GWTC-4.0 MLTP model [25] and from B-POP. Solid lines indicate the median of the reconstructed distribution, while shaded regions show the 90% C.I. obtained by varying the population parameters  $\Lambda$  that, for the MLTP model correspond to the population parameters reported in [25] while for B-POP they reduce to the mixture fraction  $\phi$ .

and isolated environments. In other words, we are “fixing” the features in the BBH mass spectrum, which carries information on the source redshifts, to the ones predicted by B-POP. Instead, [25] adopts general phenomenological models for the source mass that can account for different positions of the mass feature and therefore introduces more uncertainty in the determination of  $H_0$ . In other words, the NF model is less general than an analytical phenomenological model, but it can account for complex correlations in the mass-redshift space. Fig. 7 shows this behavior by comparing the reconstructed primary source-mass distribution from the GWTC-4.0 phenomenological Multi Peak (MLTP) model [25] with the B-POP NF model: the fiducial MLTP model has narrower 90% C.I. with respect to the B-POP model, because its only free parameter is  $\phi$ .

From the posterior on  $H_0$  and  $\phi$ , we also argue that B-POP provides a fair description of the mass and redshift distribution of currently detected GW events. This is a consequence of the fact that our posterior both supports the fiducial value of 0.37 of the mixture fraction between the two considered formation channels of BBHs, as well as the current measurements of  $H_0$  from early and late times. It is interesting to note that early-time values of  $H_0$  are supported by a higher number of dynamically assembled BBHs, while late-time values by a lower number of them. This result stems from the fact that a population more dominated by dynamically formed BBHs will display more binaries with high source mass, that can be obtained from detector masses only if the GW events are placed systematically at lower redshifts (lower  $H_0$ ).

We conclude the GWTC-4.0 results discussion with a note of caution for interpreting our results. Looking at Fig. 6, one could argue that early-time values of  $H_0$  are more consistent with the B-POP fiducial value of  $\phi = 0.37$ , and therefore more likely to be correct. However, this statement strongly relies on the assumption that *we assume* the B-POP simulation perfectly represents the population merging BBHs in the universe. This is clearly a strong assumption as B-POP is also generated using astrophysical prescriptions on which we have large uncertainties. Therefore,  $\phi$  and  $H_0$  could also be understood as a nuisance parameters for the inference that can give more flexibility to our rate model used for the inference. The effect of  $\phi$  would be to adjust the ratio of local overdensities of BBH in source mass, while the effect of  $H_0$  would be to change how this mass and redshift spectrum is converted to detector masses and luminosity distance. The most general and robust statement, from our results, is that B-POP reasonably fits the detected population of BBHs if we assume  $H_0$  closer to its early-time value, while it would need fewer BBHs formed dynamically if  $H_0$  is closer to its late-time value.

Another important point to discuss relates to the circularity of the inference. B-POP obtains BBH mergers redshift using the merger time of the binary and the redshift of formation (which is linked to the assumed Star Formation Rate). This procedure requires the assumption of a cosmological model to convert redshifts to lookback time and viceversa. In other words, the BBH merger rate computed by B-POP is  $H_0$ -dependent, and it should be generated for every  $H_0$  value. For instance, a universe with very low values of  $H_0$  would be very old and hence more binaries have time to merge, while the opposite is true for high values of  $H_0$ . In this paper, we neglect this effect, and we assume that the BBH merger rate as a function of redshift and masses does not strongly depend on values of  $H_0 \in [67, 74] \text{ km s}^{-1} \text{ Mpc}^{-1}$ . However, we underline that if the posterior has

support for extreme values of  $H_0$  and the BBH merger model strongly depends on the cosmological model, more NF should be considered.

## 6 Conclusions

We introduced a non-parametric population framework based on Normalizing Flows to model the joint source-frame masses and merger redshift distributions of binary black holes in gravitational wave cosmology and population analyses. The model replaces standard phenomenological parametric prescriptions with non-parametric, data-driven density estimators that can capture non-trivial redshift-evolving populations and complex population features.

We validated the model using a redshift-evolving mock BBH population and we showed that Normalizing Flows reconstruct the population and fully remove the systematic bias in the Hubble constant inference. This benchmark demonstrates that the Normalizing Flows population model can be used to correctly perform hierarchical Bayesian inference.

We applied the model to a synthetic astrophysical BBH catalog generated with the B-POP pipeline: the population is characterized by complex mass features and a strong redshift evolution. We modeled the isolated binaries and the dynamical formation channels with two independent and different Normalizing Flows, we combined them through a mixture coefficient and using synthetic GW observations we performed joint inference on the Hubble constant and on the dynamical formation channel fraction. We recovered the injected values without evidence for systematic biases, showing that Normalizing Flows can be used to describe astrophysically calibrated populations into the hierarchical Bayesian inference framework.

Finally, we applied the population model to real gravitational wave data from the GWTC-4.0 catalog. We used the same Normalizing Flows model we used with simulated data without any modification. We obtained constraints on the Hubble constant and formation channel mixture fraction consistent with current cosmological measurements and astrophysical expectations.

This work demonstrates that non-parametric, astrophysically calibrated population models based on Normalizing Flows provide a consistent model for gravitational wave population inference. This approach enables unbiased cosmological and population inference and it represents a promising direction for future analyses with larger gravitational wave catalogs and synthetic BBH populations.

## 7 Acknowledgments

This work is supported by ERC grant GravitySirens 101163912. Funded by the European Union. Views and opinions expressed are however those of the author(s) only and do not necessarily reflect those of the European Union or the European Research Council Executive Agency. Neither the European Union nor the granting authority can be held responsible for them. This material is based upon work supported by NSF's LIGO Laboratory which is a major facility fully funded by the National Science Foundation. F.S. has been funded by the European Union –NextGenerationEU under the Italian Ministry of University and Research (MUR) "Decreto per l'assunzione di ricercatori internazionali post-dottorato PNRR" - Missione 4 "Istruzione e Ricerca" Componente 2 "Dalla Ricerca all'Impresa" del PNRR - Investimento 1.2 "Finanziamento di progetti presentati da giovani ricercatori" - CUP D13C25000700001. M.A.S. acknowledges funding from the European Union's Horizon 2020 research and innovation programme under the Marie Skłodowska-Curie grant agreement No. 101025436 (project GRACE-BH) and from the MERAC Foundation through the 2023 MERAC prize. M.A.S. acknowledge the ACME project which has received funding from the European Union's Horizon Europe Research and Innovation programme under Grant Agreement No. 101131928.

## A Appendix

### A.1 Redshift-evolving mock catalog details

The redshift-evolving mock population used to benchmark the method is generated from a POWER LAW + PEAK [52] analytical model in which the Gaussian Peak mean evolves linearly with redshift. The merger redshift distribution follows the Madau-like rate evolution [49, 71].

The primary mass distribution follows a Power Law and a truncated Gaussian Peak, whose mean  $\mu$  evolves with redshift

$$\mu(z) = \mu_{z_0} + \mu_{z_1}z. \quad (9)$$

where  $\mu_{z_0}$  and  $\mu_{z_1}$  respectively represent the mean of the Gaussian Peak at  $z = 0$  and at  $z = 1$

The low-mass end of the distribution is smoothed over a scale  $\delta_m$ . The secondary mass is drawn conditionally on the primary mass from a smoothed Power Law distribution. The full joint

probability density can be written as

$$p(m_1, m_2, z|\Lambda) = p(m_1|z, \Lambda) p(m_2|m_1, \Lambda) p(z|\Lambda). \quad (10)$$

The parameters  $\Lambda$  used to generate the mock catalog are reported in Tab. 1.

Parameter ( $\Lambda$ )	Definition	Value
<b>Cosmology (flat <math>\Lambda</math>CDM; fixed in the mock)</b>		
$H_0$	Hubble constant [ $\text{km s}^{-1} \text{Mpc}^{-1}$ ]	67.7
$\Omega_m$	Matter density parameter	0.308
<b>Merger redshift distribution <math>p(z)</math> (Madau-like rate evolution)</b>		
$\gamma$	Low- $z$ evolution slope	4.59
$\kappa$	High- $z$ evolution slope	2.86
$z_p$	Redshift of Peak rate	2.47
<b>Primary mass distribution <math>p(m_{1s}   z)</math> (Power Law + Evolving Peak)</b>		
$\alpha$	Power Law index of the primary mass	4.09
$m_{\min}$	Minimum source-frame mass [ $M_\odot$ ]	4.98
$m_{\max}$	Maximum source-frame mass [ $M_\odot$ ]	112.5
$\mu_{z_0}$	Gaussian Peak mean at $z = 0$ [ $M_\odot$ ]	32.27
$\mu_{z_1}$	Linear redshift coefficient of the peak mean [ $M_\odot$ ]	2.5
$\sigma_{z_0}$	Gaussian Peak width [ $M_\odot$ ]	3.88
$\phi$	Fraction of events in the Gaussian Peak	0.08
$\delta_m$	Low-mass smoothing scale [ $M_\odot$ ]	3.70
<b>Secondary mass distribution <math>p(m_{2s}   m_{1s})</math></b>		
$\beta$	Power Law index of the secondary mass	-1.23

**Table 1.** Population parameters used to generate the redshift-evolving mock BBH population.

### A.2 Normalizing Flows architecture and training

In this appendix we provide the details of the implementation of the Normalizing Flows model introduced in Sec. 2. We describe the data preprocessing, model architecture, training procedure and model selection criteria.

In order to enhance the training procedure of the ZUKO [72] Normalizing Flows model, the input population samples are normalized to a fixed bounded domain  $[-b, b]$ . Given the set of input samples  $x = (m_{1s}, m_{2s}, z)$ , we compute the minimum  $x_{\max}$  and maximum  $x_{\min}$  values of each dimensions from the training dataset (80% of the total dataset). Each component is rescaled as follows:

$$x_{\text{norm}} = \frac{2b}{x_{\max} - x_{\min}}(x - x_{\min}) - b. \quad (11)$$

This choice is made to map the normalized input data within the domain over which the rational-quadratic splines of the ZUKO library are defined [57]. Outside this domain, the Normalizing Flows does not correctly model the input distribution. In this work, we fix  $b = 3.5$ . The corresponding Jacobian correction is consistently taken into account.

We use ZUKO Neural Spline Flows with a standard 3-dimensional Gaussian latent distribution. The main parameters of the flow are the number of transformations layers and the number of hidden neurons in the neural network.

We train the model by minimizing the negative log-likelihood (NLL) [56] of the training data using the Adam [73] optimizer, with a fixed learning rate and batch size. An early stopping method is used on the validation set (20% of the total dataset) to prevent overfitting.

A summary of the Normalizing Flows architectures we used for all the different population catalogs are reported in Tab. 2 and the training and validation loss curves are shown in Fig. 8, where we observe a stable convergence behaviour and no overfitting.

	Layers	Hidden neurons	Batch size	Train loss	Validation loss
Power Law	4	10	1000	1.5665	1.5663
Gaussian Peak	3	15	1000	2.5470	2.5513
B-POP isolated binaries channel	2	4	2048	3.1816	3.1830
B-POP dynamical channel	2	8	2048	2.7572	2.8048

**Table 2.** Normalizing flow architectures and training parameters used for all the population models we used in this work, in all models the learning rate and the number of iterations are respectively fixed to 0.005 and 600.

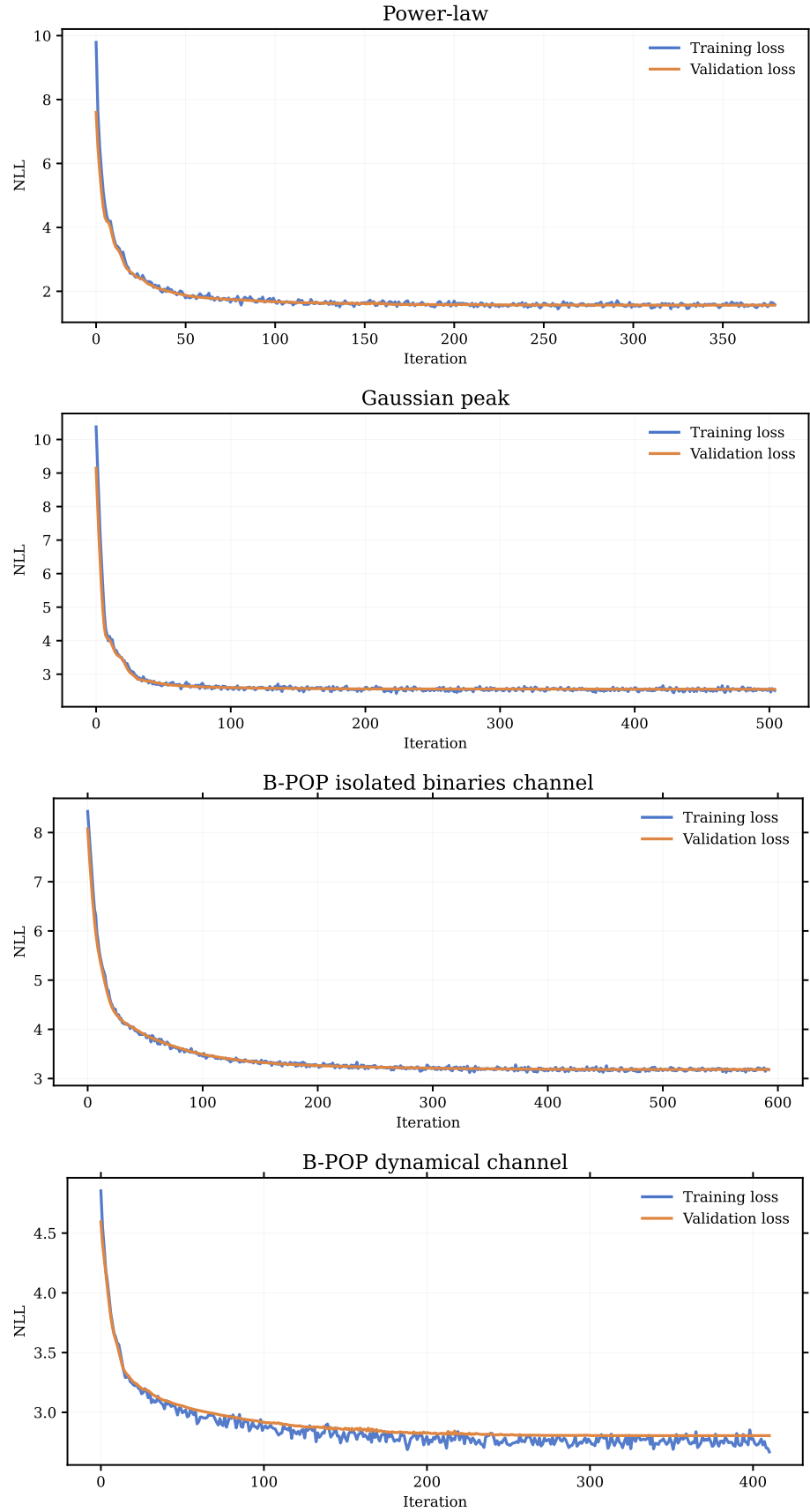


**Figure 8.** Training and validation losses as a function of the training iterations for the four population models considered in this work: the mock redshift-evolving Power Law and Gaussian Peak, the B-POP isolated binaries channel and the B-POP dynamical channel.

### A.3 Detector-frame rate for B-POP catalogs

In this appendix we discuss Eq. 8 which describes the detector-frame merger rate that uses the astrophysical synthesis catalogs generated with the B-POP pipeline and fitted with the Normalizing Flows model.

The B-POP catalogs provide BBH redshift  $z$  samples drawn from a distribution proportional to:

$$R(z) \frac{dV_c}{dz} \frac{1}{1+z}, \quad (12)$$

where  $R(z)$  is the merger rate density per comoving volume and source-frame time. This implies that, when Normalizing Flows are trained directly on the catalog samples, the resulting  $p_{\text{NF}}(m_{1s}, m_{2s}, z)$  is normalized with respect to this sampling measure. Thus, an explicit normalization is needed in order to consistently compute Eq. 3. This brings to the parametrization of the detector-frame rate for B-POP catalogs in Eq. 8, in which the total number of astrophysical mergers happening in the Universe during the observation time  $T_{\text{obs}}$  is defined as:

$$N_{\text{astro}} = T_{\text{obs}} \int dz R(z) \frac{1}{1+z} \frac{dV_c}{dz}. \quad (13)$$

## References

- [1] L. Perivolaropoulos and F. Skara, “Hubble tension or a transition of the Cepheid SnIa calibrator parameters?,” *Phys. Rev. D*, vol. 104, no. 12, p. 123511, 2021.
- [2] N. Aghanim *et al.*, “Planck 2018 results. VI. Cosmological parameters,” *Astron. Astrophys.*, vol. 641, p. A6, 2020. [Erratum: *Astron. Astrophys.* 652, C4 (2021)].
- [3] B. F. Schutz, “Determining the hubble constant from gravitational wave observations,” *Nature*, vol. 323, pp. 310–311, 1986.
- [4] D. E. Holz and S. A. Hughes, “Using gravitational-wave standard sirens,” *The Astrophysical Journal*, vol. 629, no. 1, pp. 15–22, 2005.
- [5] A. G. Riess *et al.*, “A Comprehensive Measurement of the Local Value of the Hubble Constant with  $1 \text{ km s}^{-1} \text{ Mpc}^{-1}$  Uncertainty from the Hubble Space Telescope and the SH0ES Team,” *Astrophys. J. Lett.*, vol. 934, no. 1, p. L7, 2022.
- [6] M. Fishbach *et al.*, “A Standard Siren Measurement of the Hubble Constant from GW170817 without the Electromagnetic Counterpart,” *Astrophys. J. Lett.*, vol. 871, no. 1, p. L13, 2019.
- [7] T. L. S. Collaboration, T. V. Collaboration, T. M. Collaboration, T. D. E. C. G.-E. Collaboration, and the DES Collaboration *et al.*, “A gravitational-wave standard siren measurement of the hubble constant,” *Nature*, vol. 551, pp. 85–88, 2017.
- [8] S. R. Taylor and J. R. Gair, “Cosmology with the lights off: standard sirens in the Einstein Telescope era,” *Phys. Rev. D*, vol. 86, p. 023502, 2012.
- [9] Z.-Q. You, X.-J. Zhu, G. Ashton, E. Thrane, and Z.-H. Zhu, “Standard-siren cosmology using gravitational waves from binary black holes,” *Astrophys. J.*, vol. 908, no. 2, p. 215, 2021.
- [10] M. Mancarella, E. Genoud-Prachex, and M. Maggiore, “Cosmology and modified gravitational wave propagation from binary black hole population models,” *Phys. Rev. D*, vol. 105, no. 6, p. 064030, 2022.
- [11] C. Ye and M. Fishbach, “Cosmology with standard sirens at cosmic noon,” *Phys. Rev. D*, vol. 104, no. 4, p. 043507, 2021.
- [12] J. M. Ezquiaga and D. E. Holz, “Spectral Sirens: Cosmology from the Full Mass Distribution of Compact Binaries,” *Phys. Rev. Lett.*, vol. 129, no. 6, p. 061102, 2022.
- [13] S. Mastrogiovanni, D. Laghi, R. Gray, G. C. Santoro, A. Ghosh, C. Karathanasis, K. Leyde, D. A. Steer, S. Perries, and G. Pierra, “Joint population and cosmological properties inference with gravitational waves standard sirens and galaxy surveys,” *Phys. Rev. D*, vol. 108, no. 4, p. 042002, 2023.
- [14] C. Dalang, B. Fiorini, and T. Baker, “Large scale structure prior knowledge in the dark siren method,” 10 2024.

- [15] U. Mali and R. Essick, “Striking a Chord with Spectral Sirens: Multiple Features in the Compact Binary Population Correlate with  $H_0$ ,” *Astrophys. J.*, vol. 980, no. 1, p. 85, 2025.
- [16] I. Magaña Hernandez and A. Palmese, “Spectral siren cosmology from gravitational-wave observations in GWTC-4.0,” 9 2025.
- [17] A. Palmese, J. deVicente, M. E. S. Pereira, J. Annis, W. Hartley, K. Herner, M. Soares-Santos, M. Croce, D. Hutner, I. Magaña Hernandez, A. Garcia, J. Garcia-Bellido, J. Gschwend, D. E. Holz, R. Kessler, O. Lahav, R. Morgan, C. Nicolaou, C. Conselice, R. J. Foley, M. S. S. Gill, T. M. C. Abbott, M. Agüena, S. Allam, S. Avila, K. Bechtol, E. Bertin, S. Bhargava, D. Brooks, E. Buckley-Geer, D. L. Burke, M. Carrasco Kind, J. Carretero, F. J. Castander, C. Chang, M. Costanzi, L. N. da Costa, T. M. Davis, S. Desai, H. T. Diehl, P. Doel, A. Drlica-Wagner, J. Estrada, S. Everett, A. E. Evrard, E. Fernandez, D. A. Finley, B. Flaugher, P. Fosalba, J. Frieman, E. Gaztanaga, D. W. Gerdes, D. Gruen, R. A. Gruendl, G. Gutierrez, S. R. Hinton, D. L. Hollowood, K. Honscheid, D. J. James, S. Kent, E. Krause, K. Kuehn, H. Lin, M. A. G. Maia, M. March, J. L. Marshall, P. Melchior, F. Menanteau, R. Miquel, R. L. C. Ogando, F. Paz-Chinchón, A. A. Plazas, A. Roodman, M. Sako, E. Sanchez, V. Scarpine, M. Schubnell, S. Serrano, I. Sevilla-Noarbe, J. A. Smith, M. Smith, E. Suchyta, G. Tarle, M. A. Troxel, D. L. Tucker, A. R. Walker, W. Wester, R. D. Wilkinson, J. Zuntz, and DES Collaboration, “A Statistical Standard Siren Measurement of the Hubble Constant from the LIGO/Virgo Gravitational Wave Compact Object Merger GW190814 and Dark Energy Survey Galaxies,” *The Astrophysical Journal Letters*, vol. 900, p. L33, Sept. 2020.
- [18] B. F. Schutz, “Determining the Hubble Constant from Gravitational Wave Observations,” *Nature*, vol. 323, pp. 310–311, 1986.
- [19] R. Gray *et al.*, “Joint cosmological and gravitational-wave population inference using dark sirens and galaxy catalogues,” *JCAP*, vol. 12, p. 023, 2023.
- [20] M. Oguri, “Measuring the distance-redshift relation with the cross-correlation of gravitational wave standard sirens and galaxies,” *Phys. Rev. D*, vol. 93, no. 8, p. 083511, 2016.
- [21] S. Mukherjee, B. D. Wandelt, S. M. Nissanke, and A. Silvestri, “Accurate precision Cosmology with redshift unknown gravitational wave sources,” *Phys. Rev. D*, vol. 103, no. 4, p. 043520, 2021.
- [22] S. Bera, D. Rana, S. More, and S. Bose, “Incompleteness Matters Not: Inference of  $H_0$  from Binary Black Hole-Galaxy Cross-correlations,” *The Astrophysical Journal*, vol. 902, p. 79, Oct. 2020.
- [23] S. Mukherjee, A. Krolewski, B. D. Wandelt, and J. Silk, “Cross-correlating dark sirens and galaxies: constraints on  $H_0$  from GWTC-3 of LIGO-Virgo-KAGRA,” *Astrophys. J.*, vol. 975, no. 2, p. 189, 2024.
- [24] A. G. Abac *et al.*, “GWTC-4.0: Updating the Gravitational-Wave Transient Catalog with Observations from the First Part of the Fourth LIGO-Virgo-KAGRA Observing Run,” 8 2025.
- [25] A. G. Abac *et al.*, “GWTC-4.0: Constraints on the Cosmic Expansion Rate and Modified Gravitational-wave Propagation,” 9 2025.
- [26] A. G. Abac *et al.*, “GWTC-4.0: Population Properties of Merging Compact Binaries,” 8 2025.
- [27] C. S. Ye and M. Fishbach, “The Redshift Evolution of the Binary Black Hole Mass Distribution from Dense Star Clusters,” *Astrophys. J.*, vol. 967, no. 1, p. 62, 2024.
- [28] S. Rinaldi, W. Del Pozzo, M. Mapelli, A. Lorenzo-Medina, and T. Dent, “Evidence of evolution of the black hole mass function with redshift,” *Astron. Astrophys.*, vol. 684, p. A204, 2024.
- [29] J. Heinzl, S. Biscoveanu, and S. Vitale, “Probing correlations in the binary black hole population with flexible models,” *Phys. Rev. D*, vol. 109, p. 103006, May 2024.
- [30] L. A. C. van Son, S. E. de Mink, T. Callister, S. Justham, M. Renzo, T. Wagg, F. S. Broekgaarden, F. Kummer, R. Pakmor, and I. Mandel, “The Redshift Evolution of the Binary Black Hole Merger Rate: A Weighty Matter,” *Astrophys. J.*, vol. 931, no. 1, p. 17, 2022.

- [31] E. Berti, F. Crescimbeni, G. Franciolini, S. Mastrogiovanni, P. Pani, and G. Pierra, “Inferring black hole formation channels in GWTC-4.0 via parametric mass-spin correlations derived from first principles,” 12 2025.
- [32] M. Mapelli, *Formation Channels of Single and Binary Stellar-Mass Black Holes*. 2021.
- [33] C. S. Ye and M. Fishbach, “The Redshift Evolution of the Binary Black Hole Mass Distribution from Dense Star Clusters,” *Astrophys. J.*, vol. 967, no. 1, p. 62, 2024.
- [34] I. Magaña Hernandez and A. Ray, “Beyond Gaps and Bumps: Spectral Siren Cosmology with Non-Parametric Population Models,” 4 2024.
- [35] A. M. Farah, T. A. Callister, J. M. Ezquiaga, M. Zevin, and D. E. Holz, “No Need to Know: Toward Astrophysics-free Gravitational-wave Cosmology,” *Astrophys. J.*, vol. 978, no. 2, p. 153, 2025.
- [36] M. Tagliacruzchi, M. Moresco, N. Borghi, and C. Ciapetti, “Mind the peak: improving cosmological constraints from GWTC-4.0 spectral sirens using semiparametric mass models,” 1 2026.
- [37] S. Mukherjee, “The redshift dependence of black hole mass distribution: is it reliable for standard sirens cosmology?,” *Mon. Not. Roy. Astron. Soc.*, vol. 515, no. 4, pp. 5495–5505, 2022.
- [38] C. Karathanasis, S. Mukherjee, and S. Mastrogiovanni, “Binary black holes population and cosmology in new lights: signature of PISN mass and formation channel in GWTC-3,” *Mon. Not. Roy. Astron. Soc.*, vol. 523, no. 3, pp. 4539–4555, 2023.
- [39] A. Agarwal *et al.*, “Blinded Mock Data Challenge for Gravitational-Wave Cosmology-I: Assessing the Robustness of Methods Using Binary Black Holes Mass Spectrum,” 12 2024.
- [40] G. Pierra, S. Mastrogiovanni, S. Perriès, and M. Mapelli, “Study of systematics on the cosmological inference of the Hubble constant from gravitational wave standard sirens,” *Phys. Rev. D*, vol. 109, no. 8, p. 083504, 2024.
- [41] K. W. K. Wong and D. Gerosa, “Machine-learning interpolation of population-synthesis simulations to interpret gravitational-wave observations: A case study,” *Phys. Rev. D*, vol. 100, p. 083015, Oct 2019.
- [42] S. Colloms, C. P. L. Berry, J. Veitch, and M. Zevin, “Exploring the evolution of gravitational-wave emitters with efficient emulation: Constraining the origins of binary black holes using normalizing flows,” *The Astrophysical Journal*, vol. 988, p. 189, jul 2025.
- [43] C. Plunkett, M. Mould, and S. Vitale, “Constraining population iii stellar demographics with next-generation gravitational-wave observatories,” *Phys. Rev. D*, vol. 112, p. 023039, Jul 2025.
- [44] N. Laal, S. R. Taylor, L. Z. Kelley, J. Simon, K. Gültekin, D. Wright, B. Bécsy, J. A. Casey-Clyde, S. Chen, A. Cingoranelli, D. J. D’Orazio, E. C. Gardiner, W. G. Lamb, C. Matt, M. S. Siwek, and J. M. Wachter, “Deep neural emulation of the supermassive black hole binary population,” *The Astrophysical Journal*, vol. 982, p. 55, mar 2025.
- [45] K. W. K. Wong, G. Contardo, and S. Ho, “Gravitational-wave population inference with deep flow-based generative network,” *Phys. Rev. D*, vol. 101, p. 123005, Jun 2020.
- [46] I. Mandel, W. M. Farr, and J. R. Gair, “Extracting distribution parameters from multiple uncertain observations with selection biases,” *Mon. Not. Roy. Astron. Soc.*, vol. 486, no. 1, pp. 1086–1093, 2019.
- [47] S. Vitale, D. Gerosa, W. M. Farr, and S. R. Taylor, “Inferring the properties of a population of compact binaries in presence of selection effects,” 7 2020.
- [48] G. Pierra and S. Mastrogiovanni, “Gravitational wave cosmology : an introduction,” 7 2025.
- [49] S. Mastrogiovanni, G. Pierra, S. Perriès, D. Laghi, G. Caneva Santoro, A. Ghosh, R. Gray, C. Karathanasis, and K. Leyde, “ICAROGW: A python package for inference of astrophysical population properties of noisy, heterogeneous, and incomplete observations,” *Astron. Astrophys.*, vol. 682, p. A167, 2024.

- [50] K. G. Malmquist, “On some relations in stellar statistics,” *Meddelanden fran Lunds Astronomiska Observatorium Serie I*, vol. 100, pp. 1–52, 1922.
- [51] J. M. Ezquiaga and D. E. Holz, “Spectral Sirens: Cosmology from the Full Mass Distribution of Compact Binaries,” *Phys. Rev. Lett.*, vol. 129, no. 6, p. 061102, 2022.
- [52] R. Abbott *et al.*, “Population of Merging Compact Binaries Inferred Using Gravitational Waves through GWTC-3,” *Phys. Rev. X*, vol. 13, no. 1, p. 011048, 2023.
- [53] S. Mastrogiovanni, A. Lamberts, R. Srinivasan, T. Bruel, and N. Christensen, “Inferring binary black holes stellar progenitors with gravitational wave sources,” *Mon. Not. Roy. Astron. Soc.*, vol. 517, no. 3, pp. 3432–3444, 2022.
- [54] D. Rezende and S. Mohamed, “Variational inference with normalizing flows,” in *International conference on machine learning*, pp. 1530–1538, PMLR, 2015.
- [55] I. Kobyzev, S. J. Prince, and M. A. Brubaker, “Normalizing flows: An introduction and review of current methods,” *IEEE Transactions on Pattern Analysis and Machine Intelligence*, vol. 43, pp. 3964–3979, Nov. 2021.
- [56] G. Papamakarios, E. Nalisnick, D. J. Rezende, S. Mohamed, and B. Lakshminarayanan, “Normalizing flows for probabilistic modeling and inference,” *Journal of Machine Learning Research*, vol. 22, no. 57, pp. 1–64, 2021.
- [57] C. Durkan, A. Bekasov, I. Murray, and G. Papamakarios, “Neural spline flows,” 2019.
- [58] G. Papamakarios, T. Pavlakou, and I. Murray, “Masked autoregressive flow for density estimation,” 2018.
- [59] R. Abbott *et al.*, “Constraints on the Cosmic Expansion History from GWTC-3,” *Astrophys. J.*, vol. 949, no. 2, p. 76, 2023.
- [60] R. Abbott *et al.*, “GWTC-3: Compact Binary Coalescences Observed by LIGO and Virgo during the Second Part of the Third Observing Run,” *Phys. Rev. X*, vol. 13, no. 4, p. 041039, 2023.
- [61] P. A. R. Ade *et al.*, “Planck 2015 results. XIII. Cosmological parameters,” *Astron. Astrophys.*, vol. 594, p. A13, 2016.
- [62] M. A. Sedda, M. Mapelli, M. Benacquista, and M. Spera, “Isolated and dynamical black hole mergers with B-POP: the role of star formation and dynamics, star cluster evolution, natal kicks, mass and spins, and hierarchical mergers,” *Mon. Not. Roy. Astron. Soc.*, vol. 520, no. 4, pp. 5259–5282, 2023.
- [63] M. Arca Sedda and M. Benacquista, “Using final black hole spins and masses to infer the formation history of the observed population of gravitational wave sources,” *Monthly Notices of the Royal Astronomical Society*, vol. 482, pp. 2991–3010, Jan. 2019.
- [64] M. Arca Sedda, M. Mapelli, M. Spera, M. Benacquista, and N. Giacobbo, “Fingerprints of Binary Black Hole Formation Channels Encoded in the Mass and Spin of Merger Remnants,” *The Astrophysical Journal*, vol. 894, p. 133, May 2020.
- [65] M. Arca Sedda, M. Mapelli, M. Benacquista, and M. Spera, “Isolated and dynamical black hole mergers with B-POP: the role of star formation and dynamics, star cluster evolution, natal kicks, mass and spins, and hierarchical mergers,” *Monthly Notices of the Royal Astronomical Society*, vol. 520, pp. 5259–5282, Apr. 2023.
- [66] M. Arca Sedda, F. Santoliquido, L. Paiella, B. Mestichelli, and M. Branchesi, “Isolated or dynamical? tracing black hole binary formation through the population of gravitational-wave sources,” *In preparation*, 2026.
- [67] S. Ferraiuolo, S. Mastrogiovanni, S. Escoffier, and E. Kajfasz, “Inferring astrophysics and cosmology with individual compact binary coalescences and their gravitational-wave stochastic background,” *Astron. Astrophys.*, vol. 701, p. A36, 2025.
- [68] M. Fishbach, W. M. Farr, and D. E. Holz, “The Most Massive Binary Black Hole Detections and the Identification of Population Outliers,” *Astrophys. J. Lett.*, vol. 891, no. 2, p. L31, 2020.

- [69] B. P. Abbott *et al.*, “Prospects for observing and localizing gravitational-wave transients with Advanced LIGO, Advanced Virgo and KAGRA,” *Living Rev. Rel.*, vol. 19, p. 1, 2016.
- [70] R. Essick *et al.*, “Compact binary coalescence sensitivity estimates with injection campaigns during the LIGO-Virgo-KAGRA Collaborations’ fourth observing run,” *Phys. Rev. D*, vol. 112, no. 10, p. 102001, 2025.
- [71] P. Madau and M. Dickinson, “Cosmic Star Formation History,” *Ann. Rev. Astron. Astrophys.*, vol. 52, pp. 415–486, 2014.
- [72] “Zuko documentation.” <https://zuko.readthedocs.io/stable/tutorials/basics.html>.
- [73] D. P. Kingma, “Adam: A method for stochastic optimization,” *arXiv preprint arXiv:1412.6980*, 2014.